JOURNAL OF Materials CHEMISTRY

Synthesis and ionic conductivity of pure and Co-doped lithium barium diphosphates $Li_{2-2x}Co_xBaP_2O_7$ ($0 \leqslant x \leqslant 0.06$)

Daniela Kovacheva,[a] Velin Nikolov,[a] Kostadin Petrov,[a] Rosa M. Rojas,[b] Pilar Herrero[b] and José M. Rojo*[b]

[a]*Institute of General and Inorganic Chemistry, Bulgarian Academy of Sciences, 1113 Sofia, Bulgaria*
[b]*Instituto de Ciencia de Materiales de Madrid, Consejo Superior de Investigaciones Científicas, Cantoblanco, 28049 Madrid, Spain. E-mail: jmrojo@icmm.csic.es*

Received 12th May 2000, Accepted 16th October 2000
First published as an Advance Article on the web 18th December 2000

Polycrystalline $Li_2BaP_2O_7$ was obtained by heating a stoichiometric mixture of Li_2CO_3, $BaCO_3$ and $NH_4H_2PO_4$ at 750 °C for 12 hours in an air atmosphere. Co-doped samples $Li_{2-2x}Co_xBaP_2O_7$ ($0.02 \leqslant x \leqslant 0.06$) were prepared in the same way by adding predetermined amounts of cobalt(II) acetate tetrahydrate $Co(CH_3COO)_2{\cdot}4H_2O$ in the reaction mixture. The identity of the compounds was confirmed by elemental and X-ray diffraction analysis. The ionic conductivity, ascribed to the Li^+ ion motion, was analysed by impedance measurements (frequency range: 1–10^5 Hz, temperature range: 150–600 °C) on polycrystalline pellets sintered at 720 °C for 12 hours. The ionic conductivity is discussed on the basis of the structural characteristics of the samples.

Introduction

The complex monophosphate $(PO_4)^{3-}$ and diphosphate $(P_2O_7)^{4-}$ ions have been used as building blocks for a wide variety of crystal phases with a wide spectrum of physical and chemical properties. Both crystalline and glassy monophosphate- and diphosphate-based materials have gained much interest as promising non-linear optic materials,[1] high-temperature ionic conductors,[2–5] solid electrolytes for high energy density batteries,[6] ion exchange materials, catalysts, *etc.*[7,8]

Recently the crystal structure of the lithium barium diphosphate $Li_2BaP_2O_7$ was resolved.[9] It is isostructural with $Co_2BaSi_2O_7$,[10] and contains Li^+ located in relatively narrow tunnels formed by the oxygen atoms of the diphosphate units. The aim of the present work was to study the ionic conductivity of $Li_2BaP_2O_7$ and its Co-doped materials. The information obtained could be important in two aspects. On the one hand, suppressing of the ionic conductivity is very important for the improvement of the optical characteristics of the solids. On the other hand, enhancing of the Li^+ mobility could result in the preparation of materials that could be used as solid electrolytes.

Experimental

The $Li_2BaP_2O_7$ sample was obtained from analytical reagent grade Li_2CO_3, $BaCO_3$ and $NH_4H_2PO_4$, preheated at 120 °C. The reagents were taken in stoichiometric molar ratio and ground in an agate mortar. The homogenised powder was pressed into pellets that were calcined at 600 °C for 12 h. The resulting product was reground, pelletised again, and heated from room temperature to 750 °C for 3 h, kept at this temperature for 12 h, and then cooled to room temperature at a rate of 2 °C min^{-1}. Three Co-doped samples, $Li_{2-2x}Co_x$-BaP_2O_7 ($x = 0.02$, 0.04 and 0.06), were prepared in the same manner, by adding the appropriate amounts of cobalt acetate tetrahydrate, $Co(CH_3COO)_2{\cdot}4H_2O$, to the reaction mixture.

The chemical compositions of the samples were determined by atomic emission spectrophotometric (ICP-AES) analysis. Moreover, X-ray energy dispersive analysis was carried out with a Link Isis series 300 microanalysis system, Si(Li) detector, mounted on a Jeol 2000 FX electron microscope. The samples for microanalysis were ground in acetone and dispersed on nickel grids coated with a holey carbon support film.

X-Ray diffraction (XRD) patterns were recorded at room temperature using a Siemens D-501 diffractometer with monochromatic Cu-K_α radiation ($\lambda = 1.54184$ Å). Diagrams were recorded in the step scanning mode in the $10° \leqslant 2\theta \leqslant 60°$ range, with a 0.02° (2θ) step scan and 5 s counting time. Unit cell parameters were refined by a routine least-squares program.[11]

Diffuse reflectance spectra (DRS) were recorded in the range 300–2000 nm with a Beckman UV spectrophotometer, using $BaSO_4$ as a standard.

Two-probe impedance measurements were carried out in the frequency range 1–10^5 Hz with a 1174 Solartron frequency response analyser coupled to a 1286 Solartron electrochemical interface. Pellets for electrical measurements were sintered at 720 °C for 12 h. Platinum electrodes were attached to both faces of cylindrical pellets with a platinum paste (Engelhard 6082); heating at 200 °C for 2 h and 700 °C for 4 h cured the paint. The electrical measurements were carried out in the range 150–600 °C, while the pellets were held at constant temperatures.

Results and discussion

Sample description and structural characterisation

The $Li_2BaP_2O_7$ powder shows a snow-white colour. The $Li_{2-2x}Co_xBaP_2O_7$ samples ($0.02 \leqslant x \leqslant 0.04$) have a bluish-pink tinge, which transforms to pink for the sample at $x = 0.06$. The X-ray powder diffraction patterns recorded for the doped $Li_{2-2x}Co_xBaP_2O_7$ ($0.02 \leqslant x \leqslant 0.06$) are similar to the pattern of pure $Li_2BaP_2O_7$ (Fig. 1). The indexing of the pattern for the latter compound is outlined in Table 1. The lattice parameters of the pure and doped compounds are outlined in Table 2. A lattice expansion beyond one standard deviation is observed for the most highly cobalt-doped ($x = 0.06$) sample.

The ICP-AES analysis of the pure $Li_2BaP_2O_7$ sample yielded 9.2 wt% Li_2O, 47.3 wt% BaO, and 43.4 wt% P_2O_5, values which

 DOI: 10.1039/b003816o

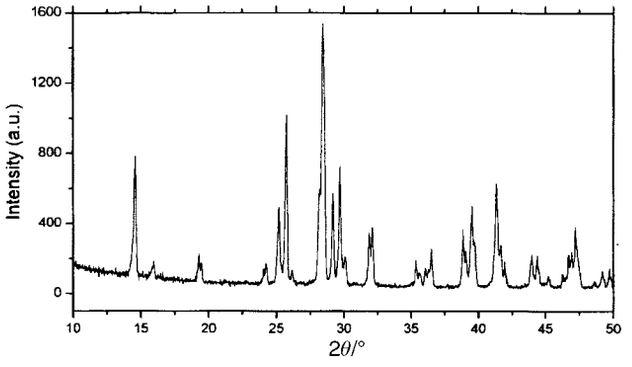

Fig. 1 X-Ray powder diffraction pattern of $Li_2BaP_2O_7$.

are in agreement with the values deduced from the formula unit: 9.19, 47.16 and 43.65 wt%, respectively. The cobalt content determined for the doped samples is also listed in Table 2. Moreover, crystals of $Li_2BaP_2O_7$ and the Co-doped samples were analysed by X-ray energy dispersive spectroscopy. Fig. 2 shows the spectra recorded for the samples at $x=0$ and 0.06. For the latter sample, in addition to the peaks corresponding to Ba (L) and P (K), the peaks corresponding to Co (K) are clearly observed. The P, Ba, and Co contents (in atom%) obtained are 61.2, 36.0, and 2.8, respectively. These values agree reasonably well with those calculated for the sample at $x=0.06$ (65.3 P, 32.7 Ba, and 2.0 atom% Co). For the sample at $x=0$, the P and Ba contents (in atom%) obtained are 65 and 35, respectively; these values being close to those calculated for $Li_2BaP_2O_7$ (66.6 P, and 33.3 atom% Ba).

$Li_2BaP_2O_7$ crystallises in the monoclinic system, space group $C2/c$.[9] The atomic coordinates and crystallographic characteristics are listed in Table 3. A representation of the crystal structure is shown in Fig. 3. The framework is built up from chains of distorted [LiO_4] corner-sharing tetrahedra, marked in dark grey, running along the $\langle 001 \rangle$ direction. Adjacent [Li–O_4] chains are linked together by $[P_2O_7]^{4-}$ groups, marked in light grey, forming cavities which contain the nine coordinated Ba atoms. In Fig. 4, another representation of the structure is depicted. Three non-equivalent Li1, Li2 and Li3 atoms marked in green, cyan and white, respectively, are present, the Li–O interatomic distances ranging from 1.95 to 2.05 Å. The Li1 atom has an extra oxygen neighbour at 2.33 Å. The non-occupied positions (labelled D1 to D7), which are available for the Li^+ ion in its motion, are also represented. The [Li1–O_4] tetrahedra, with Li1 located at the 8f positions, are separated by a non-occupied oxygen octahedron labelled D1, and by two non-occupied highly distorted oxygen tetrahedra, labelled D2. Between the [Li2–O_4] and [Li3–O_4] tetrahedra, with Li2 and Li3 situated at the 4e positions, three non-occupied oxygen face-sharing tetrahedra, labelled D3, D4 and D5, are also present. Along the c axis, D6 and D7 non-occupied positions are placed between Li3 and Li1, and Li1 and Li2, respectively. Possible conducting paths for Li^+ ions in the ab plane are marked in yellow, and along the c axis are marked in red.

Diffuse reflectance spectra recorded on the $Li_{2-2x}Co_x$-BaP_2O_7 for $0.02 \leqslant x \leqslant 0.06$ are shown in Fig. 5. Bands at ≈ 590 and ≈ 1520 nm are ascribed to tetrahedrally coordinated Co^{2+} ions ($^4T_1(P)$ and $^4T_1(F)$).[12] Bands at ≈ 470, ≈ 530 nm ($^4A_{2g}$, ^4E_g) and ≈ 1150, ≈ 1340 nm (^4E_g, $^4B_{2g}$) correspond to hexacooordinated Co^{2+}.[12] Moreover, the bands of the hexacoordinated Co^{2+} become more intense on increasing the amount of dopant. It can be interpreted that for low cobalt contents ($0.02 \leqslant x \leqslant 0.04$), Li2 and/or Li3 in tetrahedral environments are preferentially substituted by Co^{2+}. However, on increasing x, in addition to the mentioned substitution, Co^{2+} seems to occupy the octahedral D1 vacant positions. Therefore, the lithium substitution mechanism seems to change on increasing the dopant content.

Table 1 Miller indexes, interplanar spacing d (Å) and observed relative intensities of $Li_2BaP_2O_7$

$h\ k\ l$	d/Å	$(I/I_o)_{obs}$
1 1 0	6.118	9
0 2 0	6.079	73
1 1 −1	5.617	2
0 2 1	5.566	9
1 1 −2	4.607	10
1 1 2	4.562	8
1 1 −3	3.702	4
0 2 3	3.676	6
1 1 3	3.667	5
2 0 0	3.540	46
1 3 0	3.517	11
0 0 4	3.461	100
1 3 −1	3.413	1
1 3 1	3.404	5
2 0 −2	3.167	47
1 3 −2	3.143	95
2 0 2	3.137	37
1 3 2	3.128	93
2 2 0	3.059	49
0 2 4	3.008	69
2 2 −1	2.993	5
2 2 1	2.981	5
0 4 1	2.969	16
2 2 −2	2.808	28
1 3 −3	2.805	2
2 2 2	2.788	37
2 2 −3	2.562	2
0 4 3	2.538	12
1 1 −5	2.532	3
0 2 5	2.520	5
1 1 5	2.513	5
2 0 −4	2.489	10
1 3 −4	2.474	8
1 3 4	2.460	20
3 1 0	2.317	28
2 4 0	2.306	2
2 2 −4	2.304	15
3 1 −1	2.289	2
0 4 4	2.284	15
2 2 4	2.281	12
2 4 −1	2.277	26
1 5 1	2.267	22
3 1 −2	2.205	2
2 4 −2	2.193	10
3 1 2	2.189	4
1 5 −2	2.185	28
2 4 2	2.183	15
1 5 2	2.180	26
1 3 5	2.170	8
1 1 −6	2.166	18
1 1 6	2.152	12
3 1 −3	2.080	1
2 2 −5	2.063	3
1 5 −3	2.061	10
2 4 3	2.057	11
0 4 5	2.047	3
2 2 5	2.043	4
3 3 0	2.039	13
0 6 0	2.026	2
3 3 1	2.015	2
0 6 1	2.005	7
3 3 −2	1.962	8
3 3 2	1.951	4
2 0 6	1.943	18
1 3 −6	1.935	19
2 4 −4	1.926	5
1 3 6	1.924	15
2 0 6	1.923	18
3 1 4	1.915	10
2 4 4	1.912	1
3 3 −3	1.872	4
0 6 3	1.855	4
2 2 −6	1.851	7
2 2 6	1.833	11

Table 2 Composition (from ICP-EAS) and unit cell parameters (from powder X-ray diffraction data) of $Li_{2-2x}Co_xBaP_2O_7$ ($0 \leqslant x \leqslant 0.06$)

x (nominal)	x (found)	a/Å	b/Å	c/Å	β/°
0	0	7.0810(4)	12.1578(7)	13.8488(9)	90.669(3)
0.02	0.018(2)	7.0809(4)	12.1582(7)	13.8492(9)	90.668(3)
0.04	0.038(2)	7.0812(4)	12.1588(6)	13.8490(9)	90.669(3)
0.06	0.062(3)	7.0818(5)	12.1617(7)	13.8505(9)	90.667(3)

Table 3 Atomic coordinates of $Li_2BaP_2O_7$ from single crystal data[9]

Atom	Wyckoff position	x/a	y/b	z/c
Ba1	8f	0.18354(2)	0.02648(1)	0.12092(1)
P1	8f	−0.32276(8)	0.10470(5)	0.11914(4)
P2	8f	0.21983(8)	0.36975(5)	0.13481(4)
O1	8f	−0.1717(2)	0.1094(1)	0.2001(1)
O2	8f	−0.2412(2)	0.1263(1)	0.0214(1)
O3	8f	−0.5023(2)	0.1742(1)	0.1336(1)
O4	8f	−0.4107(2)	−0.0200(1)	0.1216(1)
O5	8f	0.0898(2)	0.2736(1)	0.1145(1)
O6	8f	0.2805(2)	0.3638(1)	0.2390(1)
O7	8f	0.3788(2)	0.3871(1)	0.0643(1)
Li1	8f	−0.4677(5)	0.2646(3)	0.0080(3)
Li2	4e	0	0.2333(5)	1/4
Li3	4e	0	−0.2340(4)	1/4

Space group $C2/c$ (No. 15), $a = 7.087(1)$ Å, $b = 12.163(2)$ Å, $c = 13.865(3)$ Å, $\beta = 90.70(1)°$, $Z = 8$, $V = 1195$ Å^3, $D_x = 3.61$ g cm^{-3}.

Ionic conductivity

The impedance plots ($-Z''$ *vs.* Z') recorded at two temperatures for the pellet of the undoped sample are shown in Fig. 6. These plots are typical for all the samples. At low temperatures (320 °C) an arc is observed. At higher temperatures (up to 500 °C) the arc disappears progressively and an inclined spike is observed. The resistance of the pellet can be determined from the intercept of the low frequency part of the arc, or from the intercept of the spike with the real Z' axis. Then, the overall dc conductivity of the pellet is calculated as usual. The spike, which is less inclined when gold electrodes are used instead of platinum ones, is ascribed to the electrode response, *i.e.* to blocking of Li^+ ions at the electrode surfaces. The arc, whose capacitance is in the range of 4–10 pF for all the samples, can be ascribed to the bulk or grain interior response, *i.e.* to Li^+ motion within the structure. However, to ascertain whether the arc is also affected by a grain boundary response overlapped with the grain interior one, an analysis of the imaginary part of the electric modulus as a function of the frequency was made.

The electric modulus formalism is widely used in glasses and ceramic materials because it gives information about the bulk or grain interior response and is not usually affected by blocking phenomena, *i.e.* grain boundary and electrode

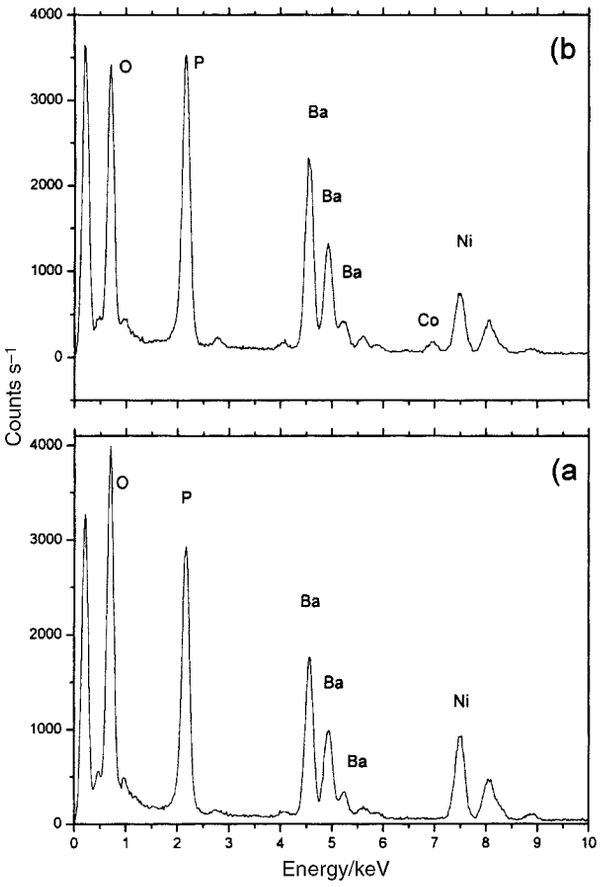

Fig. 2 Electron induced X-ray emission spectra of $Li_2BaP_2O_7$ (a), and $Li_{2-2x}Co_xBaP_2O_7$, $x = 0.06$ (b).

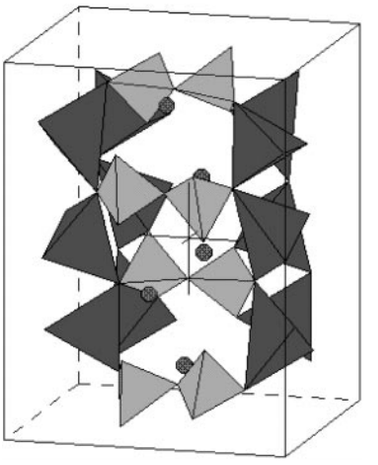

Fig. 3 A representation of the $Li_2BaP_2O_7$ structure showing the [LiO_4] tetrahedra (marked in dark grey) running parallel to the c axis. $[P_2O_7]^{4-}$ units (marked in light grey) are linking the [LiO_4] tetrahedra. Circles stand for Ba atoms.

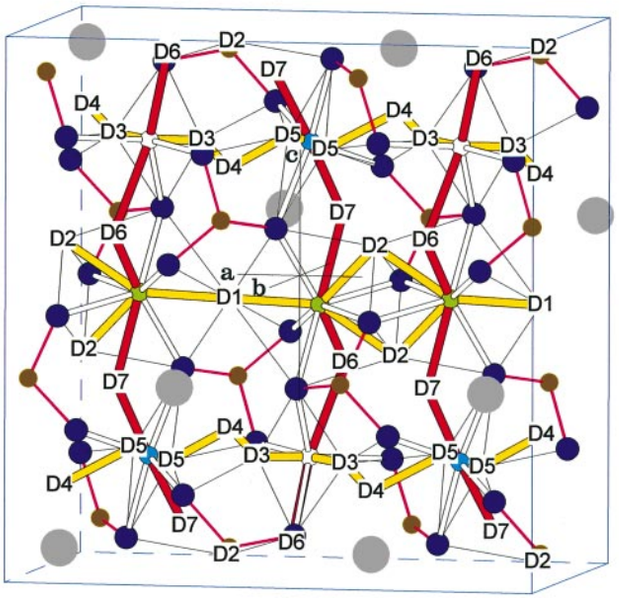

Fig. 4 Structure of the $Li_2BaP_2O_7$ showing possible conducting paths along the c axis (red) and in the ab plane (yellow). The non-occupied positions D1 to D7 are indicated. Key: dark blue, oxygen; brown, phosphorus; green, Li1; cyan, Li2; white, Li3; grey, barium.

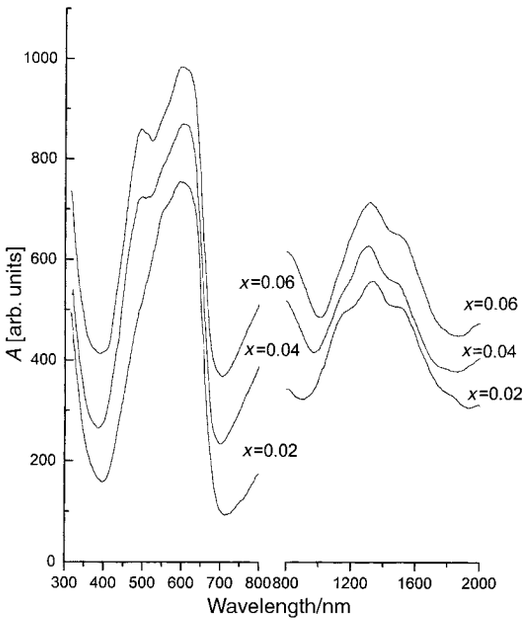

Fig. 5 Diffuse reflectance spectra of $Li_{2-2x}Co_xBaP_2O_7$ ($0.02 \leqslant x \leqslant 0.06$) in the range 300–2000 nm.

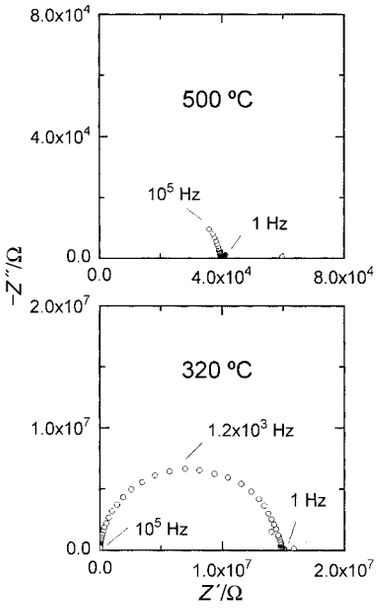

Fig. 6 Impedance plots ($-Z''$ *vs.* Z') obtained at two temperatures for a $Li_2BaP_2O_7$ pellet.

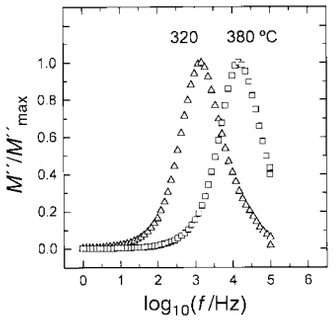

Fig. 7 Normalised imaginary electric modulus *vs.* frequency in a semi-log scale at two temperatures for $Li_2BaP_2O_7$.

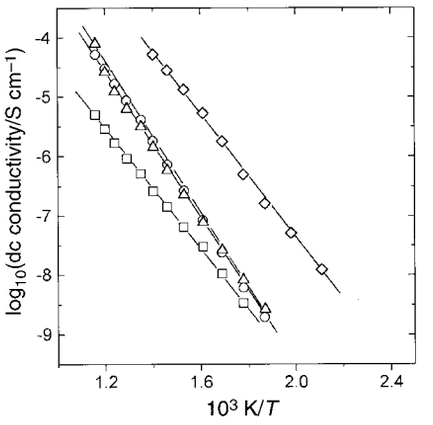

Fig. 8 Plots of the conductivity *vs.* inverse temperature for $Li_{2-2x}Co_xBaP_2O_7$: $x=0$ (circles); $x=0.02$ (triangles); $x=0.04$ (diamonds), and $x=0.06$ (squares).

response.[13] In fact, the electric modulus is proportional to $1/C$, C being the capacitance which is of the order of magnitude of pF, nF and μF for the grain interior, grain boundary, and electrode, respectively.[14,15] The imaginary part of the electric modulus (M'') as a function of the frequency shows an asymmetric peak whose position is shifted towards higher frequencies with rising temperature (Fig. 7).

The temperature dependences of the overall dc conductivity, and of the frequency at the maximum of the M'' peak, are shown in Fig. 8 and 9, respectively. The experimental conductivity and frequency data are fitted to the equations $\sigma=\sigma_0\exp(-E_\sigma/kT)$ and $f=f_0\exp(-E_f/kT)$, respectively. In these Arrhenius expressions σ_0 and f_0 are pre-exponential factors, E_σ and E_f are activation energies, k is the Boltzmann constant and T is the absolute temperature. The values of the pre-exponential factors and activation energies corresponding to the best fits together with the conductivities measured at 350 °C are outlined in Table 4. It is observed (see Table 4) that E_σ and E_f coincide within experimental error for all the pellets indicating that the impedance arcs are dominated by the grain interior response and, hence, we are dealing with the Li^+ conduction within the structure. Moreover, the high values of activation energy found for all compositions (*ca.* 1 eV) compared with the values reported[16,17] for good Li^+ conductors (0.3–0.7 eV) clearly indicate that the movement of Li^+ ions is hindered in the frameworks of $Li_2BaP_2O_7$ and Co-doped materials.

The lack of single crystals of sufficient size prevented us from determining the ionic conductivity along the three axes of the monoclinic cell. However, a comparison of the ionic con-

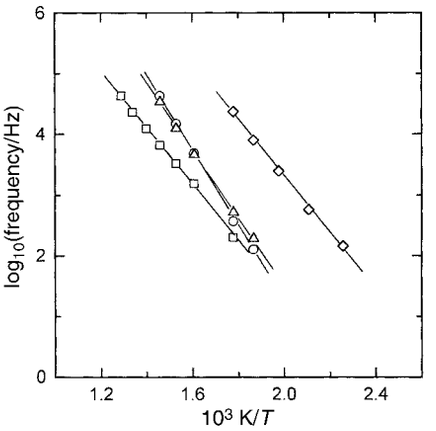

Fig. 9 Plots of the frequency at the maximum of the M'' peaks *vs.* inverse temperature for $Li_{2-2x}Co_xBaP_2O_7$: $x=0$ (circles); $x=0.02$ (triangles); $x=0.04$ (diamonds), and $x=0.06$ (squares).

Table 4 Activation energies (E_σ and E_f) and pre-exponential factors (σ_0 and f_0) deduced from the Arrhenius plots of Fig. 8 and 9. Conductivity at 350 °C is also included

x in $Li_{2-2x}Co_xBaP_2O_7$	σ_0/S cm^{-1}	E_σ/eV	$\sigma_{350\,°C}$/S cm^{-1}	f_0/Hz	E_f/eV
0	$1.0\pm0.2\times10^3$	1.24 ± 0.01	9.3×10^{-8}	$3\pm2\times10^{13}$	1.21 ± 0.04
0.02	$1.6\pm0.5\times10^2$	1.14 ± 0.02	9.6×10^{-8}	$4\pm3\times10^{12}$	1.11 ± 0.03
0.04	$1.6\pm0.6\times10^3$	1.05 ± 0.02	5.1×10^{-6}	$2\pm1\times10^{13}$	1.00 ± 0.02
0.06	2.9 ± 0.4	0.99 ± 0.01	2.8×10^{-8}	$5\pm1\times10^{10}$	0.94 ± 0.02

ductivity for the different compositions can be made. The conductivity of the pure sample increases by up to two orders of magnitude when the sample is doped with cobalt up to $x=0.04$. The pre-exponential factor (σ_0) does not change significantly but the activation energy (E_σ) decreases; so, the increase in conductivity is due to a decrease in E_σ. The decrease in E_σ can be associated with the fact that, according to the structural results already mentioned, one Co^{2+} replaces one tetrahedral Li^+. This replacement is accompanied by the formation of one Li^+ vacancy to maintain the electroneutrality of the structure. When the sample is doped with higher Co contents ($x=0.06$), the ionic conductivity decreases sharply, by *ca.* two orders of magnitude. The decrease in ionic conductivity is associated with a significant decrease in σ_0, while E_σ does not change appreciably. According to the DRS spectrum, for the sample at $x=0.06$, the Co^{2+} ions are situated, in addition to the tetrahedral Li^+ sites, at the non-occupied D1 oxygen octahedral sites, which could cause blocking of the Li^+ conducting paths.

In summary, it seems that the variation in conductivity observed can be explained on the basis of two phenomena whose effects are opposite: one, which improves the ionic conductivity, associated with the substitution for tetrahedral Li^+ by Co^{2+}, and another one, which lowers the ionic conductivity, associated with the presence of octahedral Co^{2+}. Depending on which of the two effects is dominant, the ionic conductivity can either increase or decrease upon Co doping.

Acknowledgement

The support by the CSIC and the Bulgarian Academy of Sciences through a Joint Research Project (98BG0010) is gratefully acknowledged. The Spanish authors also thank the CICYT for financial support through a project (MAT 98-0904).

References

1 M. E. Hagerman and K. R. Poppelmeyer, *Chem. Mater.*, 1995, **7**, 602.
2 H. Aono, E. Sugimoto, Y. Sadaoka, N. Amanaka and G. Adaki, *Solid State Ionics*, 1993, **62**, 309.
3 J. P. Boilot, G. Collin and P. Colomban, *J.Solid State Chem.*, 1988, **73**, 160.
4 S. Villain, E. Nigrelli and G. Nihoul, *Solid State Ionics*, 1999, **116**, 73.
5 F. Sanz, C. Parada, J. M. Rojo, C. Ruiz-Valero and R. Saez-Puche, *J. Solid State Chem.*, 1999, **145**, 604.
6 C. Delmas, A. Nadini and J. L. Subeyrou, *Solid State Ionics*, 1988, **28-30**, 419.
7 *Inorganic Ionic Exchange Materials*, ed. A. Clearfield, CRC Press, Boca Raton, FL, 1982.
8 S. Arsalane, M. Ziyad, G. Coudurier and J. C. Vedrine, *J. Catal.*, 1996, **159**, 162.
9 A. Kutoglu and R. Allmann, personal communication.
10 R. D. Adams, R. Layland, T. Datta and C. Payen, *Polyhedron*, 1993, **12**, 2075.
11 J. Macicek, PDI—A Computer Program for Powder Data Interpretation, IAM BAS, Sofia, 1988.
12 A. B. P. Lever, *Inorganic Electronic Spectroscopy*, Elsevier Science Publishers B. V., 1984, 2nd edn., ch. 6.2.7.
13 P. B. Macedo, C. T. Moynihan and R. Bose, *Phys. Chem. Glasses*, 1972, **13**, 171.
14 I. Hodge, M. D. Ingram and A. R. West, *J. Electroanal. Chem.*, 1976, **74**, 125.
15 J. Ross MacDonald, *Impedance spectroscopy. Emphasizing solid materials and systems*, John Wiley and Sons, New York, 1987.
16 A. Martinez-Juarez, C. Pecharroman, J. E. Iglesias and J. M. Rojo, *J. Phys. Chem. B*, 1998, **102**, 372.
17 V. Thangadurai, A. K. Shukla and J. Gopalakrishnan, *J.Mater. Chem.*, 1999, **9**, 739.